Eur. Phys. J. D **3**, 163–174 (1998)

THE EUROPEAN PHYSICAL JOURNAL D

Theoretical study of collisional redistribution of light near the resonance of the Ba, Sr and Mg atoms perturbed by He and Ne

E. Paul-Kwiek and E. Czuchaj[a]

Institute of Theoretical Physics and Astrophysics, University of Gdańsk , 80-952 Gdańsk, Poland

Received: 19 February 1998 / Accepted: 9 April 1998

Abstract. Absorption coefficient and polarization of collisionally redistributed fluorescence light in a range of detunings around the atomic resonance have been calculated for Ba, Sr and Mg perturbed by He and Ne. Results are obtained from fully-quantum mechanical coupled-channels calculations including the relevant ground and two excited $^1\Sigma$ and $^1\Pi$ molecular states for each diatomic. Close-coupling calculations are carried out based on the theoretical potential curves obtained by means of a pseudopotential + valence configuration-interaction (CI) technique. For accurate comparison with experiment the calculated absorption coefficients and polarizations have been thermally averaged over the collision energy. The theoretical absorption profiles and linear polarization ratios agree, in general, quite well with the available experimental data.

PACS. 34.70.+e Charge transfer – 32.80.-t Photon interactions with atoms

1 Introduction

Several papers have reported both the experimental measurements and theory of the collisional redistribution of polarized light by alkaline earth atoms perturbed by rare gases (RG). The process can, in general, be described by the equation

$$M(^1S_0) + X(^1S_0) + \hbar\omega_L \rightarrow M(^1P_1) + X(^1S_0),$$

where M represents an alkaline earth atom and X is one of the RG atoms. A laser light photon of frequency ω_L and polarization vector $\mathbf{e}_q$ is absorbed in the wings of the resonance line of the alkaline earth atom during collision with a (RG) atom. The fluorescence light of resonance frequency ω_0 observed after collision is depolarized. Study of depolarization of the fluorescence light provides information about collisional mechanisms and interaction potentials governing the atomic collisions. Since the pioneering experiments of Carlsten *et al.* [1] on collisional redistribution of light in the Sr-Ar system, a lot of experimental and theoretical studies have been devoted to both the alkali and alkaline earth atoms perturbed by rare gases. Among the alkaline earth atoms Sr [2–5] and Ba [6–10] belong to the most extensively explored systems.

In the experiments, a special attention has been given to the dependence of the depolarization rates on detuning. Theoretical developments in this field have included both full quantum close-coupling formulations and various semiclassical approaches. Omont *et al.* [11] have given a general description of the redistribution theory in applying to the case where the impact theory of spectral line broadening is valid. There has also been much interest in the study of fluorescence depolarization for excitation in the far wings of the absorption line where the impact limit does not apply. Collisional redistribution in this spectral range has been studied theoretically by several authors. The quantum optical collision approach to this problem has been formulated by Julienne and Mies [4,12–14] for the weak-coupling, binary collision case and by Kulander and Rebentrost [15,16] for the cases of zero and non-zero spin of the optically active atom. The theory fully takes into account the nonadiabatic nature of optical collisions in which multiple electronic states arising from degenerate or nearly degenerate atomic states are involved. The calculational methods are based on a coupled-channels expansion of the total wave-function of the system, thereby it is possible to treat correctly the angular momentum coupling and its change arising from absorption and emission of a photon. On the other hand classical and semiclassical treatments of optical collisions often ignore the complexity arising from angular momentum coupling including the angular momentum change of the collision system due to its interaction with the radiation field. In addition, the classical approach suffers from uncertainties in the choice of realistic trajectories needed to solve the electronic problem [5].

This paper presents the numerical results of our fully quantal close-coupling scattering calculations for Ba, Sr and Mg perturbed by light rare gases He and Ne. The calculations are based on the method formulated by Julienne and Mies [11,13]. So far quantal closed-coupled

[a] e-mail: fizec@univ.gda.pl

calculations for radiatively assisted collisions of alkaline earth atoms have been carried out for Ca-He based on model potentials [17] and for Sr-Ar using adjusted molecular potentials [4]. Contrary to that the present calculations involve the more realistic adiabatic potentials obtained by means of a pseudopotential + valence configuration interaction (CI) technique [18]. In particular the potentials for Ba-He have already been used successfully in our close-coupling calculations for the Ba($6p\,^3P_j \leftarrow 6p^1P_1$) excitation transfer and Ba($6p\,^3P_{j\rightarrow j'}$) intramultiplet transition cross-sections in collisions with He [19]. The quality of these potentials has also been supported by the recent calculation of diffusion cross-sections for barium-helium collisions [20]. The potentials for the other systems are demonstrated here for the first time. The present calculations have been motivated by the measurements of polarization of far-wing collisionally redistributed light from Sr perturbed by rare gases reported by Alford *et al.* [3] and of absorption coefficient and polarization for the Ba - (RG) atoms conducted recently by the Andersen's group [10]. The goal of this study is to reproduce their experimental results for the Ba-He(Ne) and Sr-He(Ne) pairs and to predict analogical results for Mg-He and Mg-Ne. Unfortunately, for the time being our numerical calculations for the heavy rare gases (Ar, Kr, Xe) are very time consuming, particularly on account of the averaging theoretical cross-sections over the collision energy. The following section summarizes the relevant features of the quantum theory of atomic scattering in the presence of a laser field and presents the quantum formulation of the coupled channels equations appropriate to the alkaline earth - RG atom system. Section 3 includes a brief presentation of the relevant potential curves used in the present calculations. The results and their discussion are the contents of Section 4.

2 Theory

2.1 General formulation

The quantum theory of atomic scattering in the presence of a radiation field has been presented in detail elsewhere and applied successfully to optical collisions [4,12,13,16,17]. This section summarizes the relevant features of the theory and describes the coupled channels equations appropriate to the alkaline earth - RG system. The total Hamiltonian of the molecule-field system is given by

$$H = H_{mol} + H_{rad} + H_{int}, \tag{1}$$

where H_{mol} is the Hamiltonian of the isolated alkaline earth - RG atom quasimolecule, H_{rad} is the Hamiltonian of the radiation field and H_{int} describes the interaction between the molecule and the field. The term H_{mol} is defined as

$$H_{mol} = \frac{-\hbar^2}{2\mu R^2}\frac{d}{dR}R^2\frac{d}{dR} + H_{rot} + H_{el}. \tag{2}$$

Here μ is the reduced mass of the colliding pair of atoms and R stands for the interatomic distance. H_{el} designates the electronic Hamiltonian including the nuclear repulsion and, in general, the spin-orbit interaction which in the present case does not occur since we consider only a singlet-singlet transition. The term H_{rot} is the Hamiltonian for the orbital motion of the two nuclei. The field Hamiltonian is given by

$$H_{rad} = \hbar\omega_L(a^\dagger a + 1/2), \tag{3}$$

where $a^\dagger$ and a are the photon creation and anihilation operators and ω_L is the laser frequency. The field Hamiltonian eigenvalues and eigenfunctions are defined by

$$H_{rad} \mid n\rangle = n\hbar\omega_L \mid n\rangle, \tag{4}$$

where n represents the number of photons in the laser mode.

The molecule-field interaction term is expressed as

$$H_{int} = (2\pi\hbar\omega_L\phi/c)^{1/2}\hat{\mathbf{e}}_q \cdot \mathbf{d}, \tag{5}$$

where $\hbar\omega_L\phi$ is the laser power, $\mathbf{d}$ stands for the molecular dipole moment operator, $\hat{\mathbf{e}}_q$ specifies the direction of polarization of the laser light and c is the speed of light. The field-free molecular states are eigenfunctions of the total angular momentum $\mathbf{J}$ and its space-fixed projection J_z with $\mathbf{J}=\mathbf{j}+\mathbf{l}$. Here $\mathbf{j}$ denotes the total electronic angular momentum operator and $\mathbf{l}$ is the orbital angular momentum of the nuclear motion with the quantum numbers j and l, respectively. In the considered case the radiating atom has angular momentum $j_0 = 0$ and $j = 1$ in its initial and final states, respectively, whereas the perturber atom is a structureless $^1S_0$ atom. The space-fixed quantization Z axis is taken to be along the polarization direction $\hat{\mathbf{e}}_q$ of the laser beam for linearly polarized light and along the propagation direction of the laser beam for circularly polarized light. The scattering channel states which describe the asymptotic fragments with atomic angular momentum $\mathbf{j}$ and relative angular momentum $\mathbf{l}$ given by

$$\mid jlJM\rangle = \sum_{m,m_l}(jlmm_l \mid JM) \mid jm\rangle \mid lm_l\rangle \tag{6}$$

form a convenient basis, the Hund's case-(e) basis, for expanding the total wave function for field-free scattering. Here (....| ..) denotes a Clebsch-Gordan coefficient. The expansion coefficients satisfy then the usual close-coupled equations which are diagonal in the total angular momentum J and its projection M on the space-fixed Z axis. In the presence of the radiation field J is no longer a good quantum number, a given initial J_0 being coupled to $J = J_0, J_0 \pm 1$ in the final state. The total wave function can be expanded in the molecule-field basis, consisting of products of asymptotic eigenstates of H_{mol} and eigenstates of H_{rad}

$$\psi(\mathbf{R},\mathbf{r}) = \sum_{jlnJM}\frac{1}{R}F^{j_0l_0J_0M_0}_{jlnJM}(R) \mid jlJM\rangle \mid n\rangle, \tag{7}$$

$$\langle jlJM; n'_q \mid H_{int} \mid j_0 l_0 J_0 M_0; n_q\rangle = \delta_{n'_q, n_q - 1}\left(\frac{2\pi\hbar\omega_L\phi}{c}\right)^{1/2}\frac{(2l+1)^{1/2}(2l_0+1)^{1/2}}{2J+1}$$
$$\times (J_0 1 M_0 q \mid JM)\sum_{\Omega\Omega_0}(jl\Omega 0 \mid J\Omega)(j_0 l_0 \Omega_0 0 \mid J_0\Omega_0)(J_0 1\Omega_0, \Omega-\Omega_0 \mid J\Omega)\langle j\Omega \mid d_{\Omega-\Omega_0}(R) \mid j_0\Omega_0\rangle, \quad (10)$$

$$\langle jlJM \mid H_{int} \mid j_0 l_0 J_0 M_0\rangle = \left(\frac{2\pi\hbar\omega_L\phi}{c}\right)^{1/2}(J_0 1 M_0 q \mid JM)\{(-)^{J_0+1-J}\langle A^1\Pi \mid d_1 \mid X^1\Sigma\rangle\delta_{ll_0}$$
$$+\frac{(2l+1)^{1/2}(2l_0+1)^{1/2}}{2J+1}(1l00 \mid J0)(J_0 100 \mid J0)[\langle B^1\Sigma \mid d_0 \mid X^1\Sigma\rangle - \langle A^1\Pi \mid d_1 \mid X^1\Sigma\rangle]\}. \quad (11)$$

where j_0, l_0, J_0 and M_0 refer to the initial state. The case - (e) basis functions have well-defined molecular parity with respect to inversion of all coordinates through the molecular centre of mass. The standard molecular spectroscopy parity labels are e and f for the respective basis functions of parity (-1)^J and (-1)$^{J+1}$. The expansion coefficients in equation (7) satisfy the set of close-coupled equations

$$\left[\frac{d^2}{dR^2} + k_j^2\right] F^{j_0 l_0 J_0 M_0}_{jlnJM}(R) =$$
$$\frac{2\mu}{\hbar^2}\sum_{j'l'n'J'M'} V_{jlnJM,j'l'n'J'M'}\, F^{j_0 l_0 J_0 M_0}_{j'l'n'J'M'}(R), \quad (8)$$

where $k_j = [2\mu(E-E_j)/\hbar^2]^{1/2}$ and E_j denote, respectively, the wavevector of the relative motion and electronic energy in the j-channel and E designates the total energy. In the present considerations the electronic-field asymptotic energy is chosen to be 0 for the ground state and is $-\hbar\Delta\omega$ for the excited state, where $\Delta\omega = \omega_L - \omega_0$ is the detuning from the Ba resonance frequency ($\hbar\omega_0 = E_{\rm Ba}(^1{\rm P})$-$E_{\rm Ba}(^1S)$). The matrix elements of V in equation (8), excluding the term H_{int}, defined as

$$V_{jlnJM,j'l'n'J'M'} =$$
$$\langle jlJM; n \mid \left[H_{el} + H_{rot} + H_{rad}\right] \mid j'l'J'M'; n'\rangle, \quad (9)$$

are compiled in Table 1 [4]. The adiabatic potentials W_1, W_2 and W_3 in Table 1 correspond, respectively, to the $X^1\Sigma$, $A^1\Pi$ and $B^1\Sigma$ states. They all vanish as $R\to\infty$.

The matrix elements $V_{ll'}(R)$ in Table 1 are indexed by the permitted values of channel-state quantum numbers l for a given total angular momentum J. Here for the nondegenerate $X^1\Sigma$ initial state of e-parity only $l_0 = J_0$ is permitted. The 3×3 V matrix for the threefold degenerate set of final states for a given J separates into two blocks of opposite parity: a 1×1 block for the $A^1\Pi$ state of f parity with $l = J$ and a 2×2 block for the $B^1\Sigma$ and $A^1\Pi$ states of e parity with $l = J\pm 1$. Contrary to the free-field case, the coupled equations (8) include the interaction introduced by the dipolar coupling with the radiation given by equation (5). The matrix element of H_{int} for absorption of a photon of polarization q in the space-fixed frame can be transformed to the molecular (rotating) frame as follows [15]

See equation (10) above

where Ω is the projection of $\mathbf{j}$ on the internuclear axis. In the present case $\Omega = \Lambda$, where $\mid\Lambda\rangle$ is either a $^1\Sigma(\Lambda = 0)$ or $^1\Pi(\Lambda = \pm 1)$ singlet molecular state. Finally, after the small algebra the matrix element (10) takes on the form

See equation (11) above

Note that the first term in the curly parenthesis exhibits the Hund's case (e) selection rule $l = l_0$ and the second term, which vanishes asymptotically, implies the selection rule $l = l_0 \pm 2$. The present calculations have verified the guess that the latter term is only of little consequence for the $^1S \to {}^1P$ transition, although the presence of induced-transition moments is of great importance in the case of asymptotically forbidden transitions.

For the matrix elements of H_{int} the following selection rules are satisfied: $J = J_0 + b, M = M_0 + q$ and $p = -p_0$, where p designates parity and b takes on the three possible values of the branch index b, -1, 0, +1 correspondingly to P, Q and R branches. The selection rules permit radiation-induced transitions from the e-parity initial state of total angular momentum J_0 to the two coupled final e-parity states with $J = J_0 - 1$ (P branch), to the single final f-parity state with $J = J_0$ (Q branch) and to the two coupled final e-parity states with $J = J_0 + 1$ (R branch). Although the H_{int} matrix elements depend on M and q, Julienne and Mies showed [13] that for weak radiation field this dependence can be eliminated from coupled equations by introducing reduced radiative coupling matrix elements

$$(j, l, J \parallel d^{(1)} \parallel j_0, l_0, J_0) = \frac{\langle jlJM \mid d^{(1)}_q \mid j_0 l_0 J_0 M_0\rangle}{(J1M, -q \mid J_0 M_0)}\,. \quad (12)$$

$$(j,l,J \parallel d^{(1)} \parallel j_0,l_0,J_0) = \delta_{ll_0}(-)^{l_0+1-j_0-J_0}(2j+1)^{1/2}(2J+1)^{1/2}W(j_0,j,J_0,J;1,l)(j \parallel d^{(1)} \parallel j_0), \tag{13}$$

$$f_{\mathbf{k}_0,\mathbf{k}}(j,m \leftarrow j_0,m_0;\epsilon_0,q,\omega) = \frac{2\pi i}{(k_{j_0}k_j)^{1/2}} \sum_{J_0M_0l_0m_{l_0}JMlm_l} i^{(l_0-l)}Y^*_{l_0m_{l_0}}(\hat{\mathbf{k}}_0)Y_{lm_l}(\hat{\mathbf{k}})(j_0l_0m_0m_{l_0} \mid J_0M_0)(jlmm_l \mid JM) \times S_\omega(jlJM \leftarrow j_0l_0M_0;\epsilon_0q), \tag{15}$$

Table 1. Matrix elements of $V(R)$ defined by (9) ($B(R) = \hbar^2/2\mu R^2$).

	${}^1S+{}^1\mathrm{S}$,	e-parity
$l_0 = J_0$	$W_1(R) + BJ_0(J_0+1)$	
	${}^1P+{}^1S$,	f-parity
$l = J$	$W_2(R) + BJ(J+1) - \hbar\Delta\omega$	
	${}^1P+{}^1S$,	e-parity
	$l = J-1$	$l = J+1$
$l = J-1$	$\frac{J}{2J+1}W_3 + \frac{J+1}{2J+1}W_2$ $+BJ(J-1) - \hbar\Delta\omega$	$\frac{[J(J+1)]^{1/2}}{2J+1}(W_2 - W_3)$
$l = J-1$	$\frac{[J(J+1)]^{1/2}}{2J+1}(W_2 - W_3)$	$\frac{J+1}{2J+1}W_3 + \frac{J}{2J+1}W_2$ $+B(J+1)(J+2) - \hbar\Delta\omega$

Consequently, the complete radiative scattering problem can be solved by setting up the six coupled equations, including the initial state and the five possible final channels accessible from the initial state.

If one neglects the R dependence of the electronic transition dipole moment, the reduced matrix elements can be expressed in terms of the nonvanishing asymptotic atomic transition moment

See equation (13) above

where W is a Racah coefficient. The task of scattering theory is to determine the radial functions $F(R)$ from equation (8) and extract the S-matrix elements from them by imposing the proper asymptotic boundary conditions. Assuming that all off-diagonal elements of H vanish asymptotically, one requires

$$F^{j_0l_0}_{jl}(R \to \infty) \sim \delta_{j_0j}\delta_{l_0l}e^{-i(k_{j_0}R - l_0\pi/2)} - \left(\frac{k_{j_0}}{k_j}\right)^{1/2} S(jl \leftarrow j_0l_0)e^{i(k_jR - l\pi/2)}, \tag{14}$$

where k_j is the asymptotic wavevector in a final channel j and, correspondingly, k_{j_0} refers to an initial channel j_0. The S-matrix elements can be used to predict the cross-section for any scattering experiment, for example, the cross-section for producing the final-state atoms in a particular one of their degenerate quantum states or the total cross-section for light-induced scattering from the initial to the final set of states.

2.2 Cross-sections

Standard scattering theory allows one to write the desired radiative scattering amplitudes in terms of the S-matrix elements as follows

See equation (15) above

where Y's are spherical harmonics and ϵ_0 denotes an initial relative kinetic energy. After averaging over initial states and integration over final scattering angles one finds the cross-section for the $j,m \leftarrow j_0,m_0$ transition

$$\sigma_\omega(jmq) = \frac{\pi}{(2j_0+1)k_0^2} \sum_{l_0,l,J_0,M_0} \mid \sum_J (ljM-m,m \mid JM) \times S_\omega(jlJM \leftarrow j_0l_0J_0M_0;\epsilon_0q) \mid^2 . \tag{16}$$

In the weak-field limit S_ω depends linearly on H_{int}. Making use of the Wigner-Eckart theorem one can factorize S_ω into a geometrical and dynamical part [13]

$$S_\omega(jlJM \leftarrow j_0 l_0 J_0 M_0; \epsilon_0 q) = (J1M, -q \mid J_0 M_0) \times s^b_\omega(jl \leftarrow j_0 l_0 J_0; \epsilon_0 q). \tag{17}$$

The reduced radiative S-matrix elements s^b_ω contain all the information about the optical collision in which for each branch b the transition $j, l \leftarrow j_0, l_0$ takes place from states of each initial J_0 and parity. After introducing the factorization (17) into equation (16), one obtains [4,13]

$$\sigma_\omega(jmq) = \sum_{t=j-1}^{j+1} \frac{3(j1m, -q \mid t, m-q)}{(2t+1)} \sigma^t_\omega(j), \tag{18}$$

where the transfer cross-section $\sigma^t_\omega(j)$ for the considered here case ($j_0 = 0, l_0 = J_0$) is given by

$$\sigma^t_\omega(j) = \frac{\pi}{k_0^2} \sum_{J_0} \frac{2J_0+1}{3} \sum_l \mid p^t_\omega(jlJ_0\epsilon_0) \mid^2, \tag{19}$$

with

$$p^t_\omega(jlJ_0\epsilon_0) = \sum_{b=-1}^{+1} (2J+1)^{1/2}(2t+1)^{1/2} \times W(l, j, J_0, 1; J, t) s^b_\omega(jl \leftarrow j_0 l_0 J_0; \epsilon_0 q) \tag{20}$$

and $J = J_0 + b$. Finally, the total cross-section $\sigma(\Delta\omega)$ which is independent of q for producing the final state j can be written as

$$\sigma(\Delta\omega) = \sum_{m=-j}^{j} \sigma_\omega(jmq). \tag{21}$$

Another expression for the total cross-section for producing the final $^1P_1$ state can be derived if we are interested only in lineshape and not in polarization. After averaging over the initial states m_0 and summing over the final states m one gets from equation (16) the line profile as

$$\sigma_{j \leftarrow j_0}(\Delta\omega) = \sum_{b=-1}^{1} \sigma^b_{j \leftarrow j_0}(\Delta\omega), \tag{22}$$

where

$$\sigma^b_{j \leftarrow j_0}(\Delta\omega) = \frac{\pi}{k_0^2} \sum_{l_0 l} (2J+1) \mid S^J_\omega(jlJ \leftarrow j_0 l_0; \epsilon_0) \mid^2 \tag{23}$$

with $l_0 = J_0$ and $b = 0, -1$ and 1, respectively, for the Q, P and R branches. The coupled equations (8) are solved numerically for a given choice of ϵ_0, $\Delta\omega$ and J_0 for the permitted values of b and l to get the five corresponding radiative S-matrix elements.

2.3 Spectral profile and polarization

The total radiative scattering cross-section $\sigma(\Delta\omega)$ can be related to the normalized absorption coefficient K_ω in the far spectral wings as

$$K_\omega = \frac{\langle \sigma(\Delta\omega) v \rangle}{\phi} / cm^5, \tag{24}$$

where v is relative collision velocity and the angle brackets indicate an average over the thermal velocity distribution. The radiative scattering cross-sections $\sigma_\omega(jmq)$ can be used to calculate the measured polarization ratios for either linear ($q = 0$) or circular ($q = \pm 1$) polarization experiments. The radiative excitation rate coefficients are defined as follows

$$k_\omega(m, q) = \langle \sigma_\omega(jmq) v \rangle \tag{25}$$

and the polarization ratios are calculated from them for, respectively, linear (P_s) and circular (P_c) polarization [4] as

$$P_s(\Delta\omega) = \frac{k_\omega(0,0) - k_\omega(1,0)}{k_\omega(0,0) + k_\omega(1,0)} \tag{26}$$

and

$$P_c(\Delta\omega) = \frac{k_\omega(1,1) - k_\omega(-1,1)}{k_\omega(1,1) + k_\omega(-1,1)}\,. \tag{27}$$

The numerical solution to the set of six-channel close-coupling equations yields the five S-matrix elements needed to calculate the collisional depolarization cross-sections and absorption profile for the $^1P \leftarrow {}^1S$ transition in the alkaline earth atom perturbed by the RG atom.

3 Calculations

3.1 Molecular potentials

In order to solve the set of coupled-channels equations (8) we should have the reliable adiabatic potentials $W_1(R)$, $W_2(R)$ and $W_3(R)$ for the respective $X^1\Sigma$, $A^1\Pi$ and $B^1\Sigma$ states of the M-RG system. Such potentials for Ba-He were reported earlier by Czuchaj *et al.* [18]. For the other atomic pairs the calculations have been performed very recently and the obtained results will be published shortly. The calculations are based on a non-local pseudopotential/SCF-CI scheme. In this approach the two valence electrons of the M atom are treated explicitly while the M core is simulated by the l-dependent energy-adjusted pseudopotential along with the polarization potential which includes only the dipole term. On the other hand, the RG atom is treated as a eight-valence electron system with its core simulated by scalar-relativistic l-dependent energy-consistent pseudopotential. In the molecular calculations the RG atom remains frozen in its ground-state Hartree-Fock form. Of course, such a frozen atom cannot relax in the field produced by

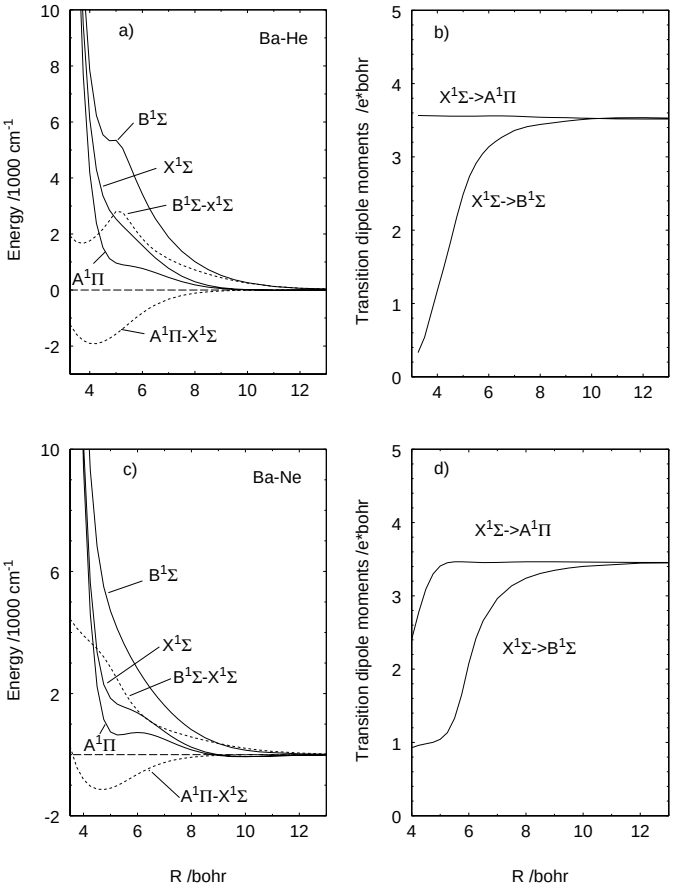

Fig. 1. Adiabatic potential curves and transition dipole moments as a function of internuclear separation for the Ba-He and Ba-Ne systems. Dotted lines show the appropriate difference potentials.

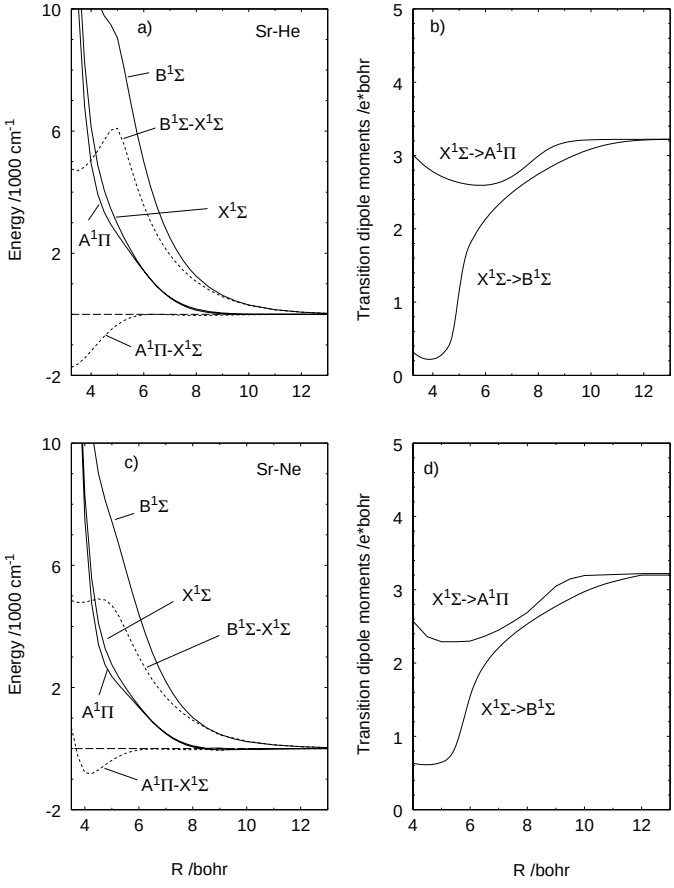

Fig. 2. Adiabatic potential curves and transition dipole moments as a function of internuclear separation for the Sr-He and Sr-Ne systems.

the alkaline earth atom. In order to account for polarization effects, the frozen RG atom is supplied with the static dipole and quadrupole polarizabilities along with the dynamical correction β_1. In addition a valence configuration-interaction (CI) treatment accounts for valence correlation effects and for the coupling between valence and core-valence correlation. The polarization potential includes a cut off function to avoid singularity when the valence electron penetrates the atomic core too deeply. The calculations are carried out in a Cartesian Gaussian basis set. First, for each internuclear separation R of the M-RG system a SCF calculation is performed to obtain the molecular Hartree-Fock orbitals for following CI calculations. A restricted CI calculation includes all single and double excitations from the M doubly occupied $ns\sigma$ valence orbital. It is essential in this approach that the calculated potentials are obtained without adjustment to any experimental data concerning the M-RG quasimolecule. Due to that the calculated interaction energies may be considered as an independent source of information on the investigated system. The theoretical potential curves for the $X^1\Sigma$, $A^1\Pi$ and $B^1\Sigma$ states of Ba, Sr and Mg interacting with He and Ne are displayed in Figures 1a, 2a, 3a and 1c, 2c, 3c, where the appropriate difference potentials are also drawn. In general, all the potential curves possess a repulsive character except for very shallow van der Waals minima at larger internuclear separations.

For Ba-He the calculated ground-state dissociation energy D_e amounts to 3.5 cm^{-1} and the equilibrium position R_e=11 bohr and, respectively, for Ba-Ne D_e=64 cm^{-1} and R_e=10 bohr. The $A^1\Pi$ potential curve is characterized by D_e=5 cm^{-1} and R_e=11 bohr for Ba-He and D_e=68 cm^{-1} and R_e=10 bohr for Ba-Ne. For the other atomic pairs considered the potential minima are shallower than the corresponding ones for Ba-He and Ba-Ne. As a rule the potential minima decrease when going through the series from Ba to Mg. Besides the potential minima are getting deep with increasing mass of the perturber. In turn the $A^1\Pi - X^1\Sigma$ and $B^1\Sigma - X^1\Sigma$ difference potentials for He and Ne calculated for a given alkaline earth atom differ not much from each other. On the other hand there exist distinct differences among the appropriate difference potentials calculated for various alkaline earth atoms. Some extrema in the difference potentials displayed in the figures give rise to a satellite structure in the line profile which lies, however, far beyond the detuning range investigated. As seen from Figure 1a, the $B^1\Sigma$ potential curve for Ba-He possesses a distinct hump near R=5 bohr which is the result of repulsion with a higher term of the same

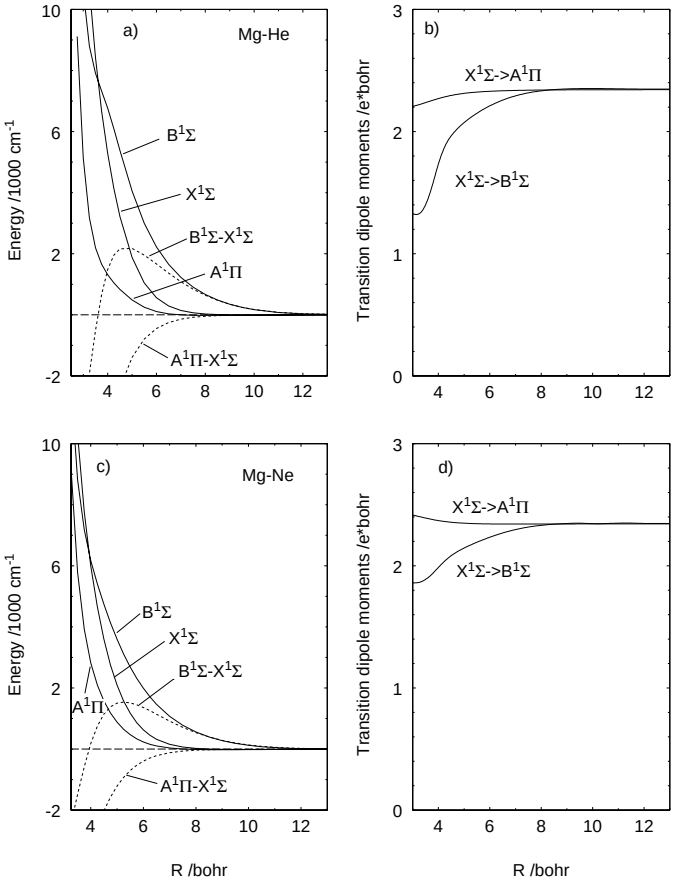

Fig. 3. Adiabatic potential curves and transition dipole moments as a function of internuclear separation for the Mg-He and Mg-Ne systems.

symmetry. Figures 1b–3b and 1d–3d show the relevant transition dipole moments calculated simultaneously with the potential curves as a function of internuclear separation. As seen the $X^1\Sigma \rightarrow A^1\Pi$ transition dipole moment for Ba-He(Ne) and Mg-He(Ne) are nearly independent of R in the entire range of internuclear separation, whereas the $X^1\Sigma \rightarrow B^1\Sigma$ dipole moment rapidly decreases for $R \ll 8$ bohr. Both the transition dipole moments for Sr-He and Sr-Ne depend considerably on internuclear separation for $R \ll 10$ bohr.

3.2 Numerical calculations

The scattering calculations were carried out with the log-derivative propagator of Johnson [21]. Separate calculations were performed for a given initial kinetic energy ϵ_0, initial total molecular angular momentum J_0 and a detuning $\Delta\omega$ from the resonance frequency at several values of temperature. In addition all the calculated cross-sections have been averaged over relative energy distribution

$$\langle \sigma_\omega(T)v \rangle = \int \sigma_\omega(\epsilon) v \epsilon^{1/2} f(\epsilon) d\epsilon \Big/ \int \epsilon^{1/2} f(\epsilon) d\epsilon \quad (28)$$

using a normalized Maxwell-Boltzmann distribution function. As to the choice of radiation flux ϕ, it can be taken as an arbitrary parameter within wide limits [4,13]. In the present calculations ϕ is taken to be 0.01 W cm^{-2} except for very small detunings lying in the impact region, where the flux had to be lessened to satisfy the condition that the Rabi frequency $\Omega_R \ll \Delta\omega$. In any case its choice should guarantee linear dependence of the reduced matrix elements s_ω on $\phi^{1/2}$. The reduced atomic matrix elements $(j \parallel d \parallel j_0)$ for the $^1P \leftarrow {}^1S$ transition are calculated simultaneously with the adiabatic potential curves and amount to 3.5014, 3.2221 and 2.3429 e·bohr, respectively, for Ba, Sr and Mg. The coupled-channels equations can be put into three separate sets of coupled equations, one for each of the three possible branches. Thus for each J_0 one obtains one set of three coupled equations for the P branch, a similar set for the R branch and a set of two coupled equations for the Q branch. The separate branch calculation appears to be more computationally efficient than the full calculation (set of six coupled equations, if all three branches are treated simultaneously).

4 Results

Any cross-section can be written as a sum of partial cross-sections $\sigma(J)$ over a wide range of the molecular angular momentum. The partial cross-sections have to be calculated for the necessary range of J_0. For a given energy and detuning the partial cross-sections were calculated from J_0=1 up to J_{0max}, where J_{0max} is large enough to ensure convergence of the J_0 summation. Typically the partial cross-section is required for several hundred J_0 values. In many cases $\sigma(J)$ is sufficiently smoothly varying function of J and interpolation using only every nth value of J can successfully be applied. There are three distinct regions of detuning for which behaviour of the partial cross-sections is different. One can speciffy the far wings, the intermediate wings and the impact region located close to the line centre. In the far-wing detuning region, absorption is predominantly to a single molecular state, to the $A^1\Pi$ state for red detunings and to the $B^1\Sigma$ state for blue detunings. The present calculations have been carried out for both the asymptotic value of the transition dipole moment and allowing for its R dependence. The obtained results (not shown here explicitly) indicate that the R dependence of the transition moment causes only a little effect on the partial cross-section. Besides its influence decreases with going from the red to the blue detunings where it disappears completely. In consequence the R dependence of the transition dipole moment may be neglected in calculations of the line profile and polarization for the resonance transition of Ba, Sr and Mg perturbed by He and Ne. In general the partial cross-section exhibits an oscillatory structure in dependence on J_0 with a growing number of maxima while going from the far wings to the line centre. For small collision energy and larger detunings the partial cross-section possesses only one maximum. With increasing energy the number of maxima grows for both large and small detunings.

Figures 4–6 show the absorption coefficient $K(\Delta\omega)$ multiplied by $(\Delta\omega)^2$ to better display the profile structure.

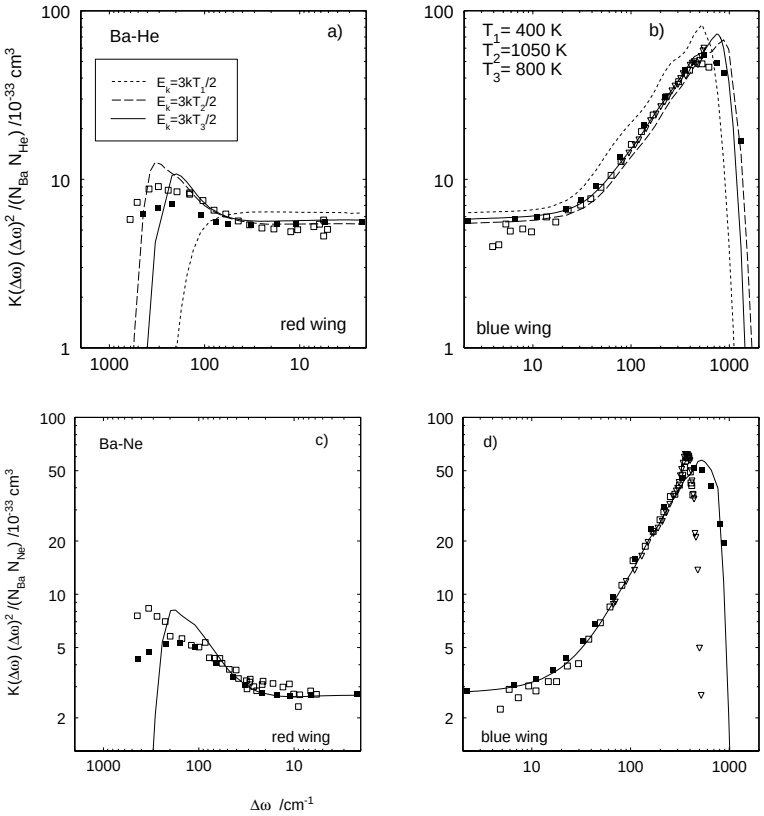

Fig. 4. Absorption coefficient multiplied by $(\Delta\omega)^2$ for the resonance transition of Ba perturbed by He and Ne as a function of detuning. Experimental data: (□) [10], (▽) [22]; (■) thermally averaged values calculated at $T = 800$ K.

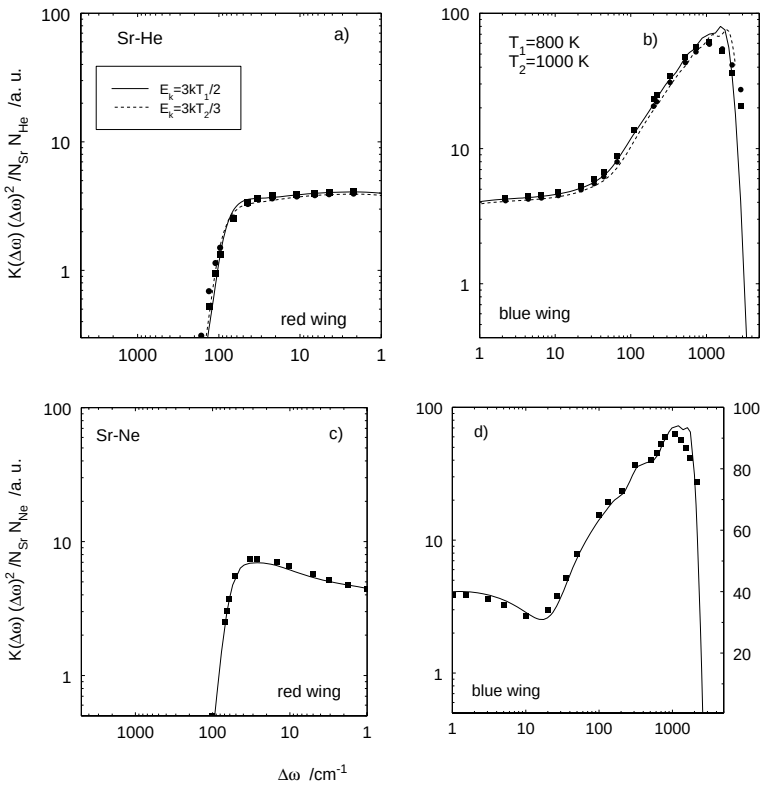

Fig. 5. Absorption coefficient multiplied by $(\Delta\omega)^2$ for the resonance transition of Sr perturbed by He and Ne as a function of detuning: (■) thermally averaged values calculated at $T = 800$ K; (•) thermally averaged points for $T = 1000$ K.

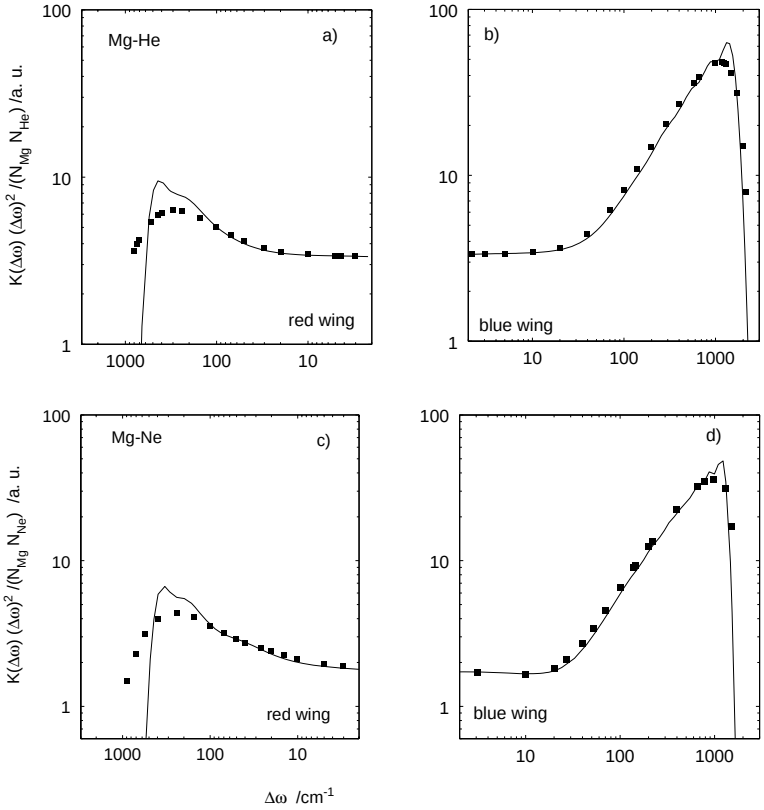

Fig. 6. Absorption coefficient multiplied by $(\Delta\omega)^2$ for the resonance transition of Mg perturbed by He and Ne calculated at $T = 800$ K as a function of detuning: (■) thermally averaged points.

In the case of Ba-He and Ba-Ne the theoretical profile has been adjusted to the experimental value at one point lying in the intermediate wing region on the blue side. In the case of Sr and Mg the theoretical line profiles are given in arbitrary units (a.u.). For accurate comparison with experiment [10,22] the calculated absorption coefficient for Ba-He and Ba-Ne has been averaged over the collision energy for $T = 800$ K which corresponds to the experimental temperature. As seen from Figure 4 the overall agreement is quite good, although some deviations occur for far-wings detunings. The theoretical profile extends beyond the experimental one in the far blue wing region and reaches a maximum at a red detuning somewhat smaller than that at which the experimental maximum occurs. The temperature effect on the line profile has been investigated for Ba-He and Sr-He. As seen from Figures 4a, 4b and 5a, 5b $K(\Delta\omega)$ is not very sensitive to T for the range of detunings shown. The theoretical line profiles for all the atomic pairs exhibit distinct deviations from the Lorentzian line shape in the far-wing regions, particularly on the blue side where a clear satellite structure develops. For Ba-He and Ba-Ne this result is supported by experiment. It is also worth noting that the calculated difference potentials for the considered systems show no extrema in the detuning region investigated and hence no satellites are predicted. The obtained result would rather indicate an alternative origin of satellite structure in the far wing regions of the resonance line of the atoms studied.

Figures 7–9 show the calculated linear polarization ratio P_s as a function of detuning. The thermally averaged theoretical results at $T = 800$ K are also compared with the corresponding measured values for Ba-He, Ba-Ne, Sr-He and Sr-Ne. The overall agreement is quite good. For Ba-He and Ba-Ne the theoretical values appear to lie somewhat above the measured points, particularly in the impact region and for red detunings. For Sr-He and Sr-Ne the agreement is even better except for the far red wing region for Sr-He, where the theoretical polarization ratio exhibits pronounced minimum near 100 cm^{-1} not observed experimentally. This disagreement seems to be connected with the rapid drop of intensity on the red side of the absorption line as seen in Figure 5. For the same reason good agreement of theory with experiment for red detunings in the case of Sr-Ne seems rather fortuitous. On the other hand the rapid drop of intensity on the red side of the spectral line for Sr-He and Sr-Ne is rather the result of deficiency of the calculated potentials for these two species. As seen from Figures 1–3, the $A^1\Pi - X^1\Sigma$ difference potentials for Sr-He and Sr-Ne essential for far red detunings differ clearly from the ones belonging to the other species. Possible deficiency of the calculated potentials for Sr-He and Sr-Ne must be ascribed to the semiempirical parameters defining the pseudopotential for the Sr atom. Figure 7 also shows the linear polarization ratio for Ba-He calculated for average energy at three different temperatures. It is seen very weak dependence of P_s on T. Finally, Figures 10 and 11 show the thermally averaged

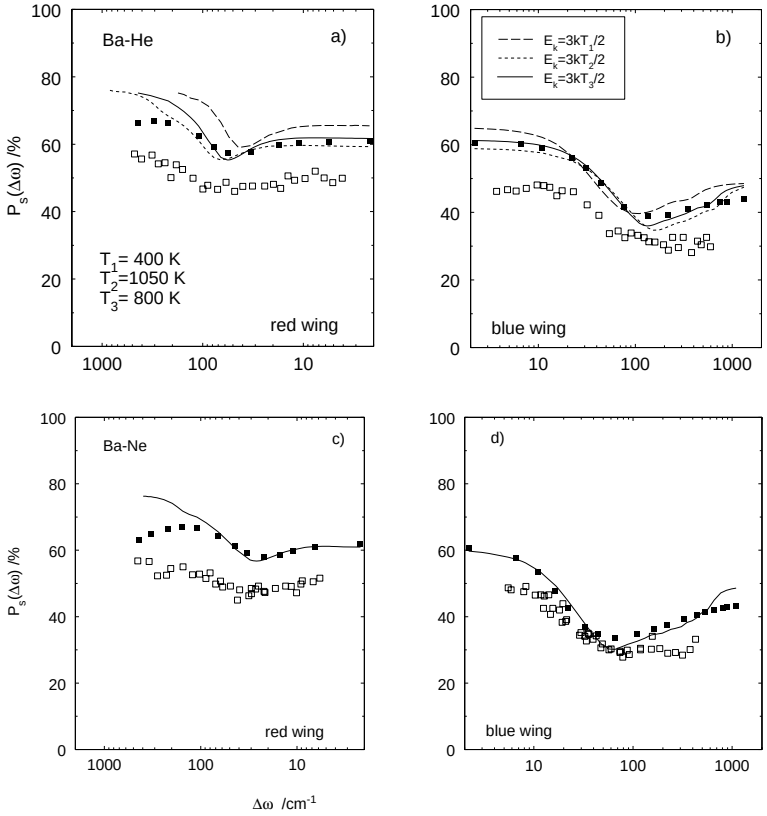

Fig. 7. Linear polarization P_s for the resonance transition of Ba perturbed by He and Ne as a function of detuning: (■) thermally averaged values calculated at $T = 800$ K; (□) experimental values [10].

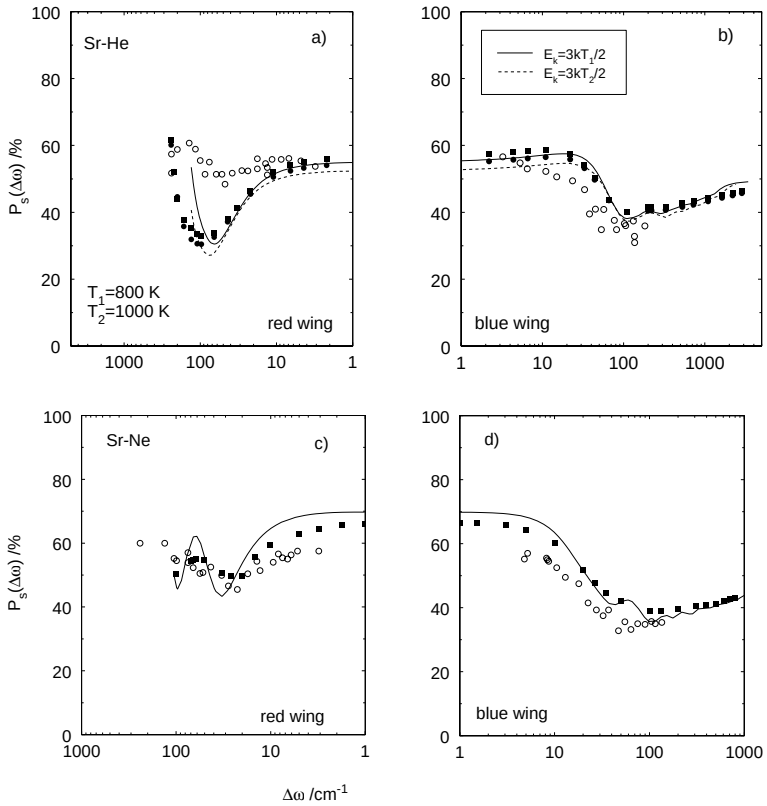

Fig. 8. Linear polarization P_s for the resonance transition of Sr perturbed by He and Ne as a function of detuning: (■) thermally averaged values calculated at $T = 800$ K; (•) thermally averaged points for $T = 1000$ K; (○) experimental points [3].

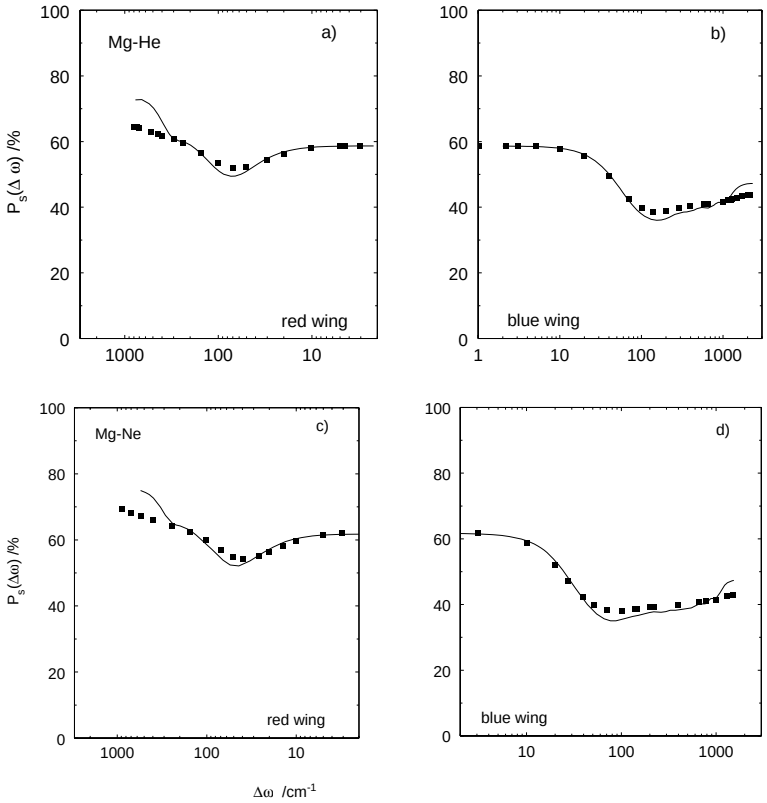

Fig. 9. Linear polarization P_s for the resonance transition of Mg perturbed by He and Ne calculated at $T = 800$ K as a function of detuning: (■) - thermally averaged points.

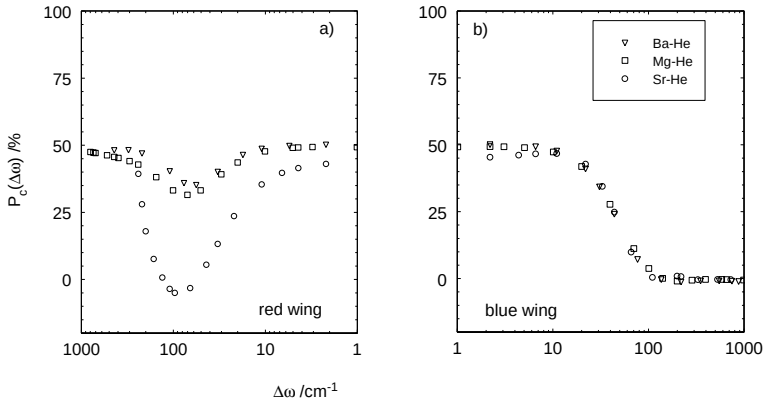

Fig. 10. Circular polarization P_c for the resonance transition of Ba, Sr and Mg perturbed by He as a function of detuning.

circular polarization ration P_c at $T = 800$ K for Ba, Sr and Mg perturbed, respectively, by He and Ne. Unfortunately, there are no P_c data for the systems studied in this paper to compare with our results. Such measurements have only been made for the Ba-Ar pair [7]. The present theoretical results for the circular polarization agree, however, quite well with overall prediction of theory. According to the theory [23], the red-wing circular polarization decreases as the detuning leaves the impact region, reaches a minimum at a detuning in the intermediate wings region and then increases with further increase of detuning. For the blue wing the circular polarization decreases with increasing detuning from the impact region and falls off to zero for higher detunings. As seen from Figures 10 and 11 our theoretical results verify the prediction of the theory in the entire range of detunings.

5 Conclusion

In this article we have demonstrated fully quantum close-coupling calculations of the absorption coefficient and polarization of fluorescence light in dependence on detuning

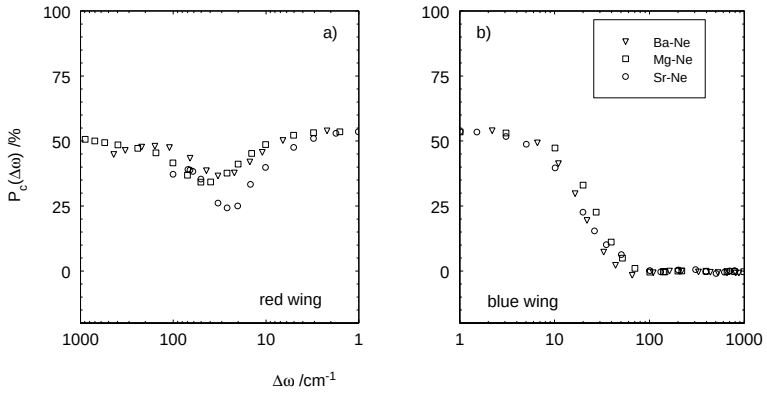

Fig. 11. Circular polarization P_c for the resonance transition of Ba, Sr and Mg perturbed by Ne as a function of detuning.

for the Ba, Sr and Mg atoms perturbed by He and Ne. The calculations are based on the theoretical adiabatic potential curves obtained by means of a pseudopotential SCF-CI technique. Particular attention was paid to reproducing the recently published experimental data for the Ba-RG systems obtained in the Andersen's laboratory. Our thermally averaged absorption coefficients for Ba-He and Ba-Ne agree very well with the experimental ones over a wide range of detunings except for far wing regions. We have also obtained good agreement for linear polarization for these species. Our thermally averaged points lie only slightly above the experimental points. For the circular polarization there are no data to compare with our results. However, overall behaviour of the calculated circular polarization agrees very well with the prediction of theory. The present calculations support both the quality of our potential curves and the coupled-channels technique in understanding of collisional redistribution of light in gases under single collision conditions and in the weak radiation field limit. Further calculations involving heavy RG atoms are in progress.

The present work was supported by the University of Gdansk (Grant No. BW/5400-5-0304-7). We are also gratful to Dr T. Orlikowski for providing us with the computer code.

References

1. J.L. Carlsten, A. Szöke, M.G. Raymer, Phys. Rev. A **15**, 1029 (1977).
2. P. Thomann, K. Burnett, J. Cooper, Phys. Rev. Lett. **45**, 1325 (1980).
3. W.J. Alford, K. Burnett, J. Cooper, Phys. Rev. A **27**, 1310 (1983).
4. P.S. Julienne, F.H. Mies, Phys. Rev. A **34**, 3792 (1986).
5. R.J. Bieniek, P.S. Julienne, F.J. Rebentrost, J. Phys. B **24**, 5103 (1991).
6. W.J. Alford, N. Andersen, K. Burnett, J. Cooper, Phys. Rev. A **30**, 2366 (1984).
7. W.J. Alford, N. Andersen, M. Belsley, J. Cooper, D.M. Warrington, K. Burnett, Phys. Rev. A **31**, 3012 (1985).
8. M.S. Belsley, J. Cooper, Phys. Rev. A **35**, 1013 (1987).
9. M.S. Belsley, J. Coutts, J. Cooper, Phys. Rev. A **38**, 3781 (1988).
10. S.Y. Ni, W. Goetz, H.A.J. Meijer, N. Andersen, Z. Phys. D **38**, 303 (1996).
11. A. Omont, E.W. Smith, J. Cooper, Astrophys. J. **175**, 185 (1972).
12. P.S. Julienne, Phys. Rev. A **26**, 3299 (1982).
13. P.S. Julienne, F.H. Mies, Phys. Rev. A **30**, 831 (1984).
14. L.L. Vahala, P.S. Julienne, M.D. Havey, Phys. Rev. A **34**, 1856 (1986).
15. K.C. Kulander, F. Rebentrost, Phys. Rev. Lett. **51**, 1262 (1983).
16. K.C. Kulander, F. Rebentrost, J. Chem. Phys. **80**, 5623 (1984).
17. B. Pouilly, J. Chem. Phys. **95**, 5861 (1991).
18. E. Czuchaj, F. Rebentrost, H. Stoll, H. Preuss, Chem. Phys. **196**, 37 (1995).
19. E. Paul-Kwiek, E. Czuchaj, Molec. Phys. **91**, 113 (1997).
20. R.K. Namiotka, E. Ehrlacher, J. Sagle, M. Brewer, D.J. Namiotka, A.P. Hickman, A.D. Streater, J. Huennekens, Phys. Rev. A **54**, 449 (1996).
21. B.R. Johnson, J. Comput. Phys. **13**, 445 (1973).
22. T. Maeyama, H. Ito, H. Chiba, K. Ohmoni, K. Ueda, Y. Sato, J. Chem. Phys. **97**, 9492 (1992).
23. K. Burnett, J. Cooper, Phys. Rev. A **22**, 2027; **22**, 2044 (1980).